An automated field spectrometer system for studying VIS, NIR and SWIR anisotropy for semi-arid savanna

Huber, Silvia; Tagesson, Torbern; Fensholt, Rasmus

Published in:
Remote Sensing of Environment

DOI:
10.1016/j.rse.2014.06.007

2014

Document Version:
Publisher's PDF, also known as Version of record

Remote Sensing of Environment 152 (2014) 547–556

Contents lists available at ScienceDirect

Remote Sensing of Environment

journal homepage: www.elsevier.com/locate/rse

An automated field spectrometer system for studying VIS, NIR and SWIR anisotropy for semi-arid savanna

Silvia Huber [a,*], Torbern Tagesson [b], Rasmus Fensholt [b]

[a] DHI GRAS A/S, Geocenter, Øster Voldgade 10, DK-1350 Copenhagen, Denmark
[b] Department of Geosciences and Natural Resource Management, University of Copenhagen, Øster Voldgade 10, DK-1350 Copenhagen, Denmark

ARTICLE INFO

Article history:
Received 14 December 2013
Received in revised form 17 June 2014
Accepted 19 June 2014
Available online 8 August 2014

Keywords:
anisotropy
hyperspectral
multi-angular
Senegal
spectro-directional
vegetation indices

ABSTRACT

This paper presents the Dahra field spectrometer system (DAFIS) sited in Senegal, West Africa. DAFIS is a unique system that automatically measures the spectro-directional reflectance properties of a semi-arid savanna in the spectral range of 350–1800 nm, daily from sunrise to sunset. The instrumental setup allows studying surface anisotropy for different phenological phases. First data retrieved from the Dahra field spectrometer system show distinctive patterns of spectrally dependent anisotropic behavior: during the rainy season normalized reflectance was highest around solar noon for small off-nadir observation angles but for observations of large off-nadir angles highest values were found in the morning or evening hours (both forward and backward scatter direction). Anisotropy factors corresponding to MODIS, SPOT and SEVIRI red, near-infrared (NIR) and shortwave-infrared (SWIR) sensor response functions indicated little influence of the anisotropic behavior for savanna but vegetation indices including red/NIR (NDVI) and NIR/SWIR (SIWSI) were found to be sensitive to the view angle (NDVI and SIWSI varied by 5 and 41 %, respectively). Surprisingly, the influence from differences in shading (analyzed by measurements from forward and backward scatter direction) did not have a noticeable impact on the indices (0.2 % and 0.5 % difference for NDVI and SIWSI in the backward and forward scatter direction, respectively). The presented data show the large potential of continuous time series collected with the DAFIS system for monitoring of plant spectro-directional behavior in semi-arid African savanna for quantitative evaluation of satellite or airborne remote sensing data or development of new Earth Observation (EO) based indices and algorithms to monitor vegetation status or stress.

1. Introduction

A large number of remote sensing systems are currently in place to observe the Earth's surface from spaceborne and airborne platforms. A consistent comparison between products is thereby difficult because Earth Observation (EO) data are highly influenced by anisotropic effects (Weyermann, Damm, Kneubühler and Schaepman, 2013). Regular spectral multi-angular measurements from ground-based systems are rare but they could help validating and correcting EO data, better understanding upscaling issues, designing EO-based indices and models for environmental monitoring. Only a handful sites exist where automated hyperspectral field data have been collected.

Gamon, Cheng, Claudio, MacKinney, and Sims (2006), Gamon, Rahman, Dungan, Schildhauer, and Huemmrich (2006) report on an automated tram system consisting of a dual-detector spectrometer mounted on a robotic cart for measuring reflectance in the range of approx. 310–1130 nm over the diurnal cycle. The system was installed within a chaparral ecosystem in California, USA. Leuning, Hughes, Daniel, Coops, and Newnham (2006) describe a multi-angle spectrometer (MAS) system mounted on a tower in Australia. The system measures hourly spectral reflectance of a forest canopy between 300 and 1150 nm at four azimuth angles throughout the year. Hilker, Coops, Nesic, Wulder, and Black (2007); Hilker, Nesic, Coops, and Lessard (2010) describe an automated spectral data collection system named AMSPEC (Automated Multiangular Spectro-radiometer for Estimation of Canopy reflectance) which is installed in Canada. The AMSPEC system is mounted on a tower and measures year round spectral reflectance of a forest canopy between 350 and 1200 nm under different viewing and sun angle conditions. The system is able to sample spectra in a near 360° view around the tower with adjustable viewing zenith angle (Hilker et al., 2007).

Yet, none of the described systems provide measurements in the shortwave-infrared (SWIR) spectral range, which has been shown to be valuable for vegetation water content retrieval (Tucker, 1980). Canopy water stress is the most common limitation to photosynthesis and plant primary productivity at the global scale (Nemani et al., 2003). Near-infrared (NIR)/SWIR based indices have been shown to be promising for monitoring canopy water content (Carter, 1991; Ceccato, Flasse, Tarantola, Jacquemoud, & Grégoire, 2001; Fensholt & Sandholt, 2003; Gao, 1996; Tucker, 1980) which is a key indicator for drought assessments in dryland ecosystems (Wang & Qu, 2007; Zhao

* Corresponding author. Tel.: +45 45169487.
E-mail address: huber.silvia@gmail.com (S. Huber).

http://dx.doi.org/10.1016/j.rse.2014.06.007
0034-4257/

et al., 2013). Visible (VIS), NIR and SWIR sensitivity to variations in soil moisture, leaf water content and bidirectional reflectance distribution function (BRDF) for vegetated surfaces has been studied using radiative transfer models (Jacquemoud et al., 2009; Latifovic, Cihlar, & Chen, 2003; Wang, Qu, Hao, & Zhu, 2008). However, the effect of bidirectional reflectance factor (BRF) variations on EO-based vegetation indices is currently not well documented for different plant functional types and ecosystems. There is a need for ground-based continuous multi-angular measurements suitable for a direct comparison and validation of EO data products from polar orbiting instruments with sensors influenced by day-to-day variations in sun-target-sensor geometry impacting on the derived vegetation products (Fensholt, Huber, Proud, & Mbow, 2010; Fensholt, Sandholt, Proud, Stisen, & Rasmussen, 2010) or products that provide a characterization of surface anisotropy used to both determine global land surface albedos and nadir view-angle-corrected reflectance (MODIS Surface Reflectance BRDF/Albedo) (Lucht, Schaaf, & Strahler, 2000).

In this paper we present data and the setup of an automated multi-angular field spectrometric system situated in the semi-arid Senegalese Sahel. Unique to this system is that it provides regular spectral measurements of a region with only sparse ground data coverage and that not only VIS and NIR but also the SWIR spectral range is measured. The semi-arid Sahel is characterized by extreme inter-annual variability in rainfall (Nicholson, Dezfuli, & Klotter, 2012) thereby posing one of the biggest obstacles to the achievement of food security in the region (Kandji, Verchot, & Mackensen, 2006). Due to the highly variable climate in the Sahel, temporal continuity in spectro-directional measurements is important to get representative measures on the one hand and to capture key transitions in ecosystem behavior associated with disturbance and stress on the other hand (Gamon, Cheng, Claudio, MacKinney, & Sims, 2006; Gamon, Rahman, Dungan, Schildhauer, & Huemmrich, 2006).

The objective of this paper is twofold: (1) to outline the measurement scheme and set up of the automated multi-angular field spectrometric system and (2) to present first analyses of spectral anisotropy in the spectral range from VIS to SWIR. Two different seasons were analyzed to investigate the impact of anisotropic data on the use of two well-known vegetation indices covering together both VIS/NIR/SWIR wavelengths.

2. Materials and methods

2.1. The Dahra field site

The field spectrometer system has been installed at the Dahra field site in the semi-arid northern part of Senegal (15.40° N, 15.43° W) (Fensholt & Sandholt, 2005; Fensholt, Sandholt, & Stisen, 2006) (Fig. 1). The savanna ecosystem found at the area is similar to many other parts of the Sahel (Hanan, Prevost, Diouf, & Diallo, 1991). Fine-leaved annual grasses with a maximum height of 60 cm, such as *Schoenefeldia gracilis, Dactyloctenium aegupticum, Aristida mutabilis*, and *Cenchrus biflores* dominate the herbaceous layer in the region (Valenza & Diallo, 1972), but widely spaced perennial grasses with a maximum height of 80 cm can also be found (Ridder, Stroosnijder, Cisse, & van Kelulen, 1982). Tree and shrub canopy cover generally do not exceed 5% and are dominated by two species: *Balanites aegyptiaca* and *Boscia senegalensis* (Diallo, Diouf, Hanan, Ndiaye, & Prévost, 1991). The soil type can be characterised as poorly developed formed on sandy parent material of dunes or fluvial deposits (less than 3% clay). The rainy season stretches from July to October and precipitation is sparse and intermittent with annual totals ranging from 300 to 500 mm and is thus typical for the Sahelian environment. The Dahra site, where measurements of climate, radiometry and fluxes have been recorded since 2002, is characterized by a uniform vegetation cover (Fig. 1) within a radius of at least 3 km from the fieldwork site to reduce uncertainty in the point to pixel comparison (Fensholt, Huber, Proud, & Mbow, 2010; Fensholt, Sandholt, Proud, Stisen, & Rasmussen, 2010; Fensholt et al., 2006).

2.2. The Dahra field spectrometer system (DAFIS)

The DAFIS was installed in 2011 and consists of two ASD FieldSpec3® spectrometers (ASD Inc., Colorado, USA). While one is mounted on a 12 m mast pointing to the land surface (ASD-FS_{target}), the other one is mounted on a 2 m high stand pointing to a Spectralon panel under a glass dome (ASD-FS_{ref}) (Labsphere Inc., New Hampshire, USA) (Fig. 2). Measurements are acquired at 15-minute intervals (corresponding to the Meteosat Second Generation (MSG) acquisition scheme) from sunrise to sunset and over the entire calendar year. The instruments are

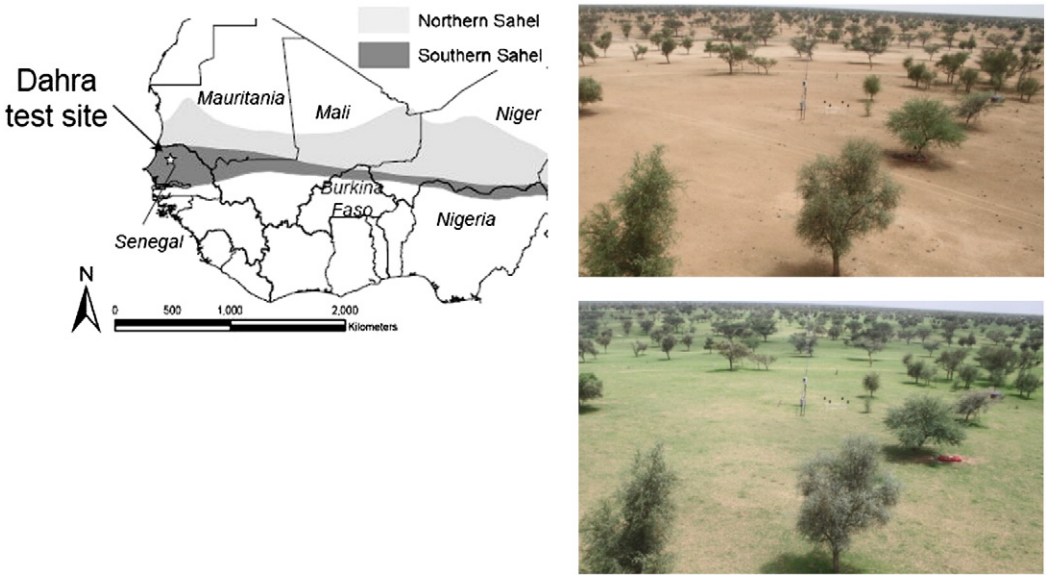

Fig. 1. Location of the Dahra field site (Senegal) in the semi-arid Sahel. The north-southern boundaries of the Sahel can be defined by the 100 mm and 600–800 mm isohyets, respectively. Photographs show the grassland savanna at the Dahra site (taken from south) in the dry season (upper photograph, taken on July 1, 2013) and at the very beginning of the rainy season (lower photograph, taken on August 1, 2013) showing predominantly annual grasses and a tree cover of less than 5 %.

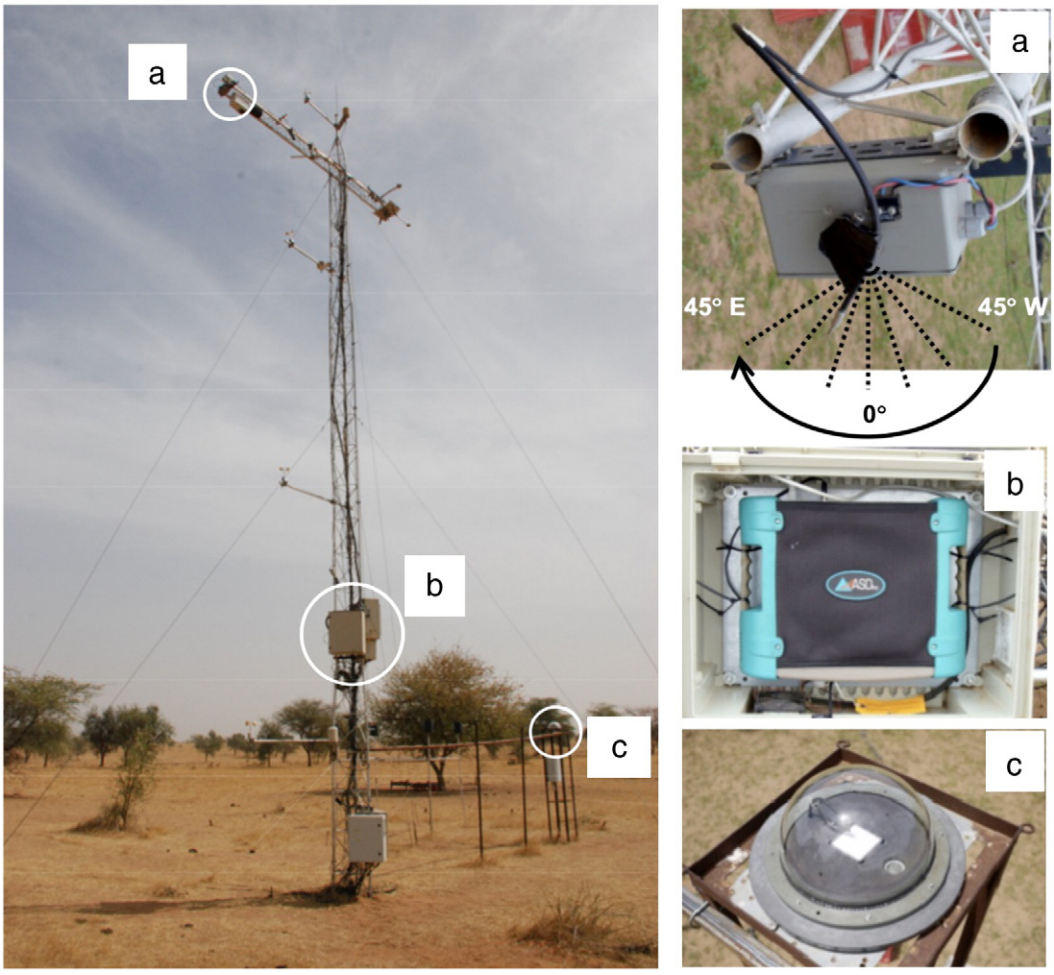

Fig. 2. Mast at the Dahra field site with the position of (a) the stepper motor controlling the optical fiber for multi-angular target measurements, (b) one of the two ASD field spec and (c) the Spectralon panel under the glass dome for white reference measurements.

controlled by custom-made Matlab scripts. The Matlab code controls the movement of the Trinamic (TMCM-1110) motor and saves the recorded ASD data. The TMCM-1110 is a stepper motor controller module that can be setup with a TMCL (TrinamicMotionControlLanguage) firmware (TMCL™ firmware manual). To move the motor to the seven positions, we use the ROR (rotate right) command and the MVP (move to position) command to move the motor back to the original position. All the commands are sent via the Matlab code to the motor controller by the serial port (COM1) in binary mode.

2.2.1. Radiometer setup for target measurements

The radiometer mounted on the mast (ASD-FS_{target}) provides radiance measurements from the land surface from seven different viewing zenith angles (nadir, 15°, 30°, 45° in eastern and western directions) with viewing azimuth angles of 270° and 90°, respectively. The stepper motor is designed to control the positioning of the optical fiber (Fig. 2a). With the radiometer having a 25° instantaneous field of view (IFOV) and being mounted at 10.5 m height, the corresponding ground instantaneous field of view (GIFOV) at nadir is circular with a radius of 2.34 m. The sampled area is ca. 17 m^2. For off-nadir observation angles the sensor's footprint becomes elliptical (Table 1).

2.2.2. Radiometer setup for white reference measurements

A Reflective Cosine Receptor (RCR, no.A124700) is used to measure full-sky-irradiance (Fig. 2c). The RCR includes a white Spectralon panel (Labsphere Inc., New Hampshire, USA), a fiber optic mount assembly and a protective dome of 22 cm in horizontal diameter. The RCR assembly is a commercial product designed for long-term installation (Analytical Spectral Devices Inc., 1999). The Spectralon measurements are used as an irradiance reference for calculating reflectance.

2.2.3. Measurement sequence and protocol

Each measurement sequence starts with the ASD-FS_{ref} from which an optimization is conducted followed by a dark current (DC) measurement. Optimization adjusts the sensitivity of the ASD detectors according to the specific illumination conditions at the time of measurement to avoid saturation of the detectors due to changing levels of downwelling irradiance. Dark current is the measurement noise stemming from a relatively small electric current generated by the thermal electrons within the ASDs that flows through the devices even when no photons

Table 1
Change of the ground instantaneous field of view (GIFOV) relative to the observation angle. Note that the major half axis of the GIFOV is changing asymmetrically in the along (east-west) and across direction from the center point.

Observation angle [°]	Major half axis along sensor track [m]	Major half axis across sensor track [m]	Sampled area [m^2]
0	2.34	2.34	17.22
15	2.67	2.37	18.52
30	3.58	2.77	23.34
45	6.02	3.83	36.22

are entering the devices. Therefore, DC has to be measured and subtracted from the measurements at 350-1000 nm on a band-by-band basis while the SWIR array (1000–1800 nm) has an automatic DC correction (each radiometer consists of two detectors, one array in the visible-NIR domain (350–1000 nm) and a second array in the SWIR range (1000–1800 nm)). After the DC of ASD-FS_{ref} is determined, the white reference is measured. Then, the ASD-FS_{target} radiometer is optimised and subsequently the DC current is measured, followed by target measurements from seven different viewing zenith angles. Finally, the ASD-FS_{ref} is again optimised, the DC current measured and a white reference measurement taken. For both radiometers, 30 scans are averaged to one measurement to improve the signal-to-noise ratio (white reference, DC and at each of the seven target measurements). Remaining poor quality measurements caused by unfavorable weather conditions or irregular technical issues were filtered by summing total solar irradiance in the range 350–1800 nm, calculating the fraction between the total solar irradiance in the beginning and the end of the measurement sequence, and rejecting all measurements with a fraction range outside of 0.95–1.05. Completion of a measurement sequence takes less than a minute in total. Data are stored as Digital Numbers (DNs) on a field computer and can be later converted into physical values following the method in Analytical Spectral Devices Inc. (1999).

2.3. Data handling

2.3.1. Sensor calibration

Before and after each rainy season the two ASD instruments are calibrated against each other. Both fiber optic cables are aligned pointing to a Spectralon panel so that both sensors measure incoming irradiance. Following Hilker et al. (2010), corrected reflectance (ρ) can be estimated from:

$$\rho = \rho_{raw} \frac{E_{irradiance}}{E_{control}} \quad (1)$$

where ρ_{raw} is raw reflectance, $E_{irradiance}$ is the Spectralon irradiance measured with the ASD-FS_{target}, $E_{control}$ is the Spectralon irradiance measured with the ASD-FS_{ref}.

2.3.2. Temperature effects on the measured reflectance

We tested the sensitivity of the instrument to temperature by altering the temperature inside the ASD box during DOY 13 and 15 in 2013. While altering the temperature, we did a similar relative sensor calibration setup as described above. The measurements were conducted in 5 minute intervals under clear sky conditions; the illumination conditions did not change during the inter-calibration procedure. Then the reflectance of the Spectralon panel was measured. Also offset dependency on temperature between instruments was checked by taking measurements in complete darkness. During the measurements, the temperature in the boxes containing each of the two ASDs was altered by placing buckets with ice and boiling water inside the boxes for 2 hours, to cover most of the temperature range (30–50 °C) observed at the Dahra site.

We did not see any sensitivity to temperature for the ASD set up (Fig. 3). The measured variability is within the measurement error of the ASD instruments (Analytical Spectral Devices Inc., 1999). Additionally, there were no temperature effects for the offset of the ASD instruments, while the average offset range was very small (<0.0003 W m^{-2}) (Fig. 3 b). It was not possible to alter the temperature inside the ASD box during the temperature experiment to cover the full range at which the ASDs operate. However, we captured the majority of the range where we expect the measurements to be sensitive to temperature. Mainly the lower temperatures were not captured, but those conditions mirror the "normal" operation range of the ASDs. In the VNIR range the ASD instruments work with silicon detectors which were reported to be very stable with respect to temperature (Walthall, Roujean, & Morisette, 2000) and the SWIR InGaAs photodiodes are thermoelectrically cooled (Analytical Spectral Devices Inc., 1999).

2.4. Data analysis

2.4.1. Normalized reflectance

We investigated the spectral anisotropic behavior of the savanna for the rainy and the dry season to assess the influence of the canopy structure on reflectance signatures and vegetation indices calculated from VIS, NIR and SWIR information. Fifteen days at the peak of the rainy season in 2011 (DOY 237–251) and during the dry season in 2012 (DOY 71–85) were selected. Only days with full data coverage were used to prevent bias in the results from including days with an incomplete dynamic range of measurements. The median reflectance was extracted for every 15 minutes, each measured angle and wavelength. Then, the ratio between the median reflectance for each wavelength and the daily average reflectance for each wavelength was calculated. This gives a fraction of how the reflectance spectra vary over the day in relation to the daily average (in the following referred to as the normalized reflectance).

2.4.2. Anisotropy factor

In order to assess the influence of the satellite spectral bandwidth upon the target's anisotropy we spectrally resampled the original ASD spectra to approximate the response of MODIS, SEVIRI (aboard MSG) and SPOT Vegetation sensors by using their spectral response functions (Fig. 4).

The bandwidths of the three sensors' Red, NIR and SWIR bands are shown in Table 2.

These three sensors were selected because they all cover the VIS, NIR and SWIR spectral range and data from these sensor systems are widely used. We have chosen to calculate the anisotropy factor (ANIF) (Eq. (2))

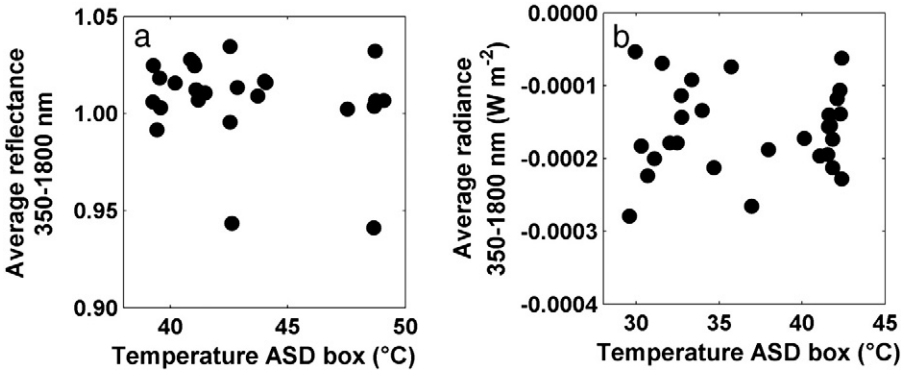

Fig. 3. The temperature effect on the reflectance spectra from measurements done at DOY 13 and 15, January 2013; a) average reflectance 350–1800 nm of a Spectralon panel against temperature inside the ASD box, and b) average radiance during complete dark conditions against temperature inside the ASD box.

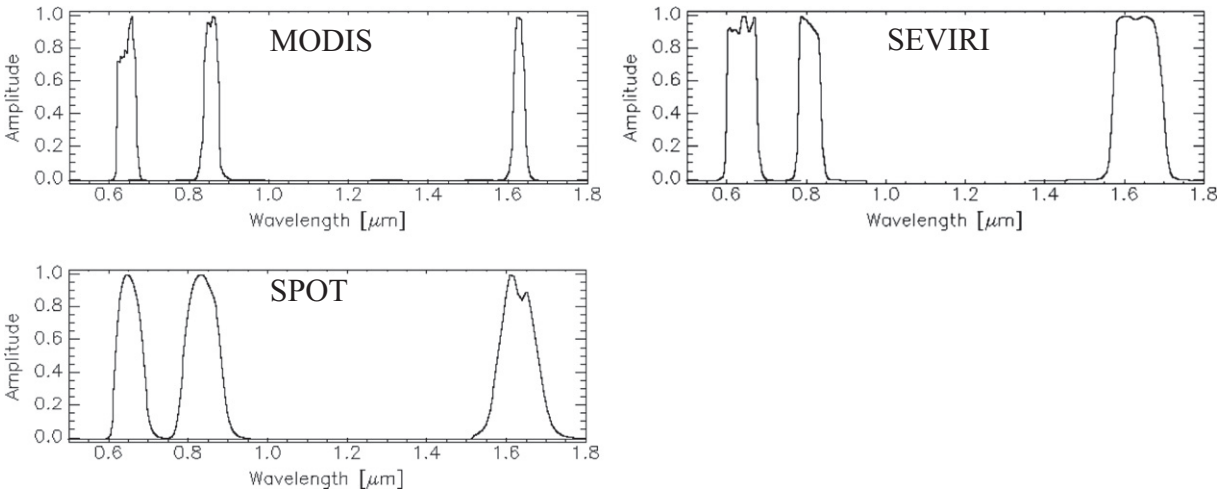

Fig. 4. Spectral response functions of MODIS, SEVIRI and SPOT for red, NIR and SWIR wavelength ranges.

from the resampled spectra to compare anisotropy between the different sensors. The ANIF can be defined as the portion of radiation reflected into a specific view direction relative to the nadir reflectance (Sandmeier, Muller, Hosgood, & Andreoli, 1998):

$$ANIF(\lambda,\theta_s,\varphi_s,\theta_v,\varphi_v)=\frac{\rho(\lambda,\theta_s,\varphi_s,\theta_v,\varphi_v)}{\rho_0(\lambda,\theta_s,\varphi_s)}[\text{dimensionless}], \quad (2)$$

where, ρ = bi-directional reflectance factor, ρ_0 = nadir reflectance factor, λ = wavelength, θ = zenith angle, = azimuth angle, s = illumination direction, and v = viewing direction.

3. Results and discussion

3.1. Reflectance measurements

The grassland savanna at the Dahra field site has a pronounced seasonality, which is also reflected in the selected spectral signatures (Fig. **5**). The average spectrum for the rainy season shows the typical features of green vegetation with a prominent green peak, increased chlorophyll absorption at 680 nm and increased reflectance in the NIR wavelengths and a peak at about 1600 nm. The reflectance spectrum of the dry season compares rather with a signature measured for soil, illustrating that no green vegetation remained (no green peak). The higher reflectance between 1400 and 1800 nm for the dry season as compared to the rainy season shows that plant water is a good absorber of SWIR energy: the higher the leaf water content, the lower the SWIR reflectance because of fewer interfaces of intercellular spaces where incident energy is scattered (Zarco-Tejada, Rueda, & Ustin, 2003).

3.2. Normalized reflectance

The spectro-directional behavior of the vegetation cover during the rainy season is shown in Fig. 6. The figure shows distinctively that anisotropic effects are wavelength dependent and more pronounced with increasing observation angles. The noise visible at 1190 and 1450 nm is related to the atmospheric water absorption bands.

The anisotropy found in the data of the nadir, 15ºW and 15ºE observations is similar, with highest normalized reflectance at around 13:00 (local solar noon) in the VIS and SWIR range (Fig. 5). In these high absorbing spectral ranges (e.g., blue and red wavelengths) less radiation is available for further scattering which tends to reduce the contrast between shadowed and illuminated areas within the canopy and hence BRDF effects (Hapke, DiMucci, Nelson, & Smythe, 1996; Kimes, 1983). In contrast, the NIR range shows a rather isotropic behavior due to increased multiple scattering (Kimes, 1983). The high normalized reflectance for nadir observations at solar noon for VIS and SWIR is related to the relatively sparse fractional green vegetation cover. Well visible when looking from nadir is the soil background and dry plant material (characterized by higher reflectance values in the VIS and the SWIR as compared to photosynthetic active material, see Fig. 5) thereby increasing the measured signal for low solar zenith angles around local solar noon.

With increasing off-nadir viewing angles the highest normalized reflectance is measured in the morning (45°W) and evening hours (45°E) because in erectophile canopies only the illuminated top part of the canopy can be seen while the amounts of shadowed fractions of lower canopy components are hidden (Kimes, 1983). This phenomenon is visible in Fig. 5 (30°E/W and 45°E/W). It is particularly so when viewed from the direction of illumination (Kimes, 1984), e.g, in the morning hours for a westward looking sensor when the sensor measures back-scattered light. The solar zenith angle reaches 45° degrees shortly before 10 and after 16 o'clock (local solar time), respectively, leading to a hotspot situation around those times for the most extreme off-nadir angles. For larger off-nadir viewing angles, anisotropy was also observed for NIR in contrary to the nadir and 15°E/W observations.

Interestingly, our observations revealed very high forward scattering (exceeding the normalized reflectance values observed for the backward scattering) in particular for 30° and 45° westward-looking off-nadir angles for evening hours (also data from the eastward-looking angles show forward scattering in the morning hours, but with lower normalized reflectance values). Possibly, the waxy coatings of the plants seen under these specific angles lead to extreme specular (mirror-like) surface reflectance which substantially enhances forward scattering (Govaerts, Jacquemoud, Verstraete, & Ustin, 1996; Grant, 1987). Also diffuse irradiance is causing higher forward scattering (Privette & Vermote, 2004) which corresponds well with general high loads of aerosols and water vapor in the semi-arid Sahel causing significant diffuse irradiance for increased solar zenith angles (longer path through

Table 2
Red, near infrared (NIR) and shortwave infrared (SWIR) bandwidths for MODIS, SEVIRI and SPOT, respectively.

Sensor	Red [nm]	NIR [nm]	SWIR [nm]
MODIS	620-670 (50)	841-876 (35)	1628-1652 (24)
SEVIRI	560-710 (150)	740-880 (140)	1500-1780 (280)
SPOT	610-680 (70)	780-890 (110)	1580-1750 (170)

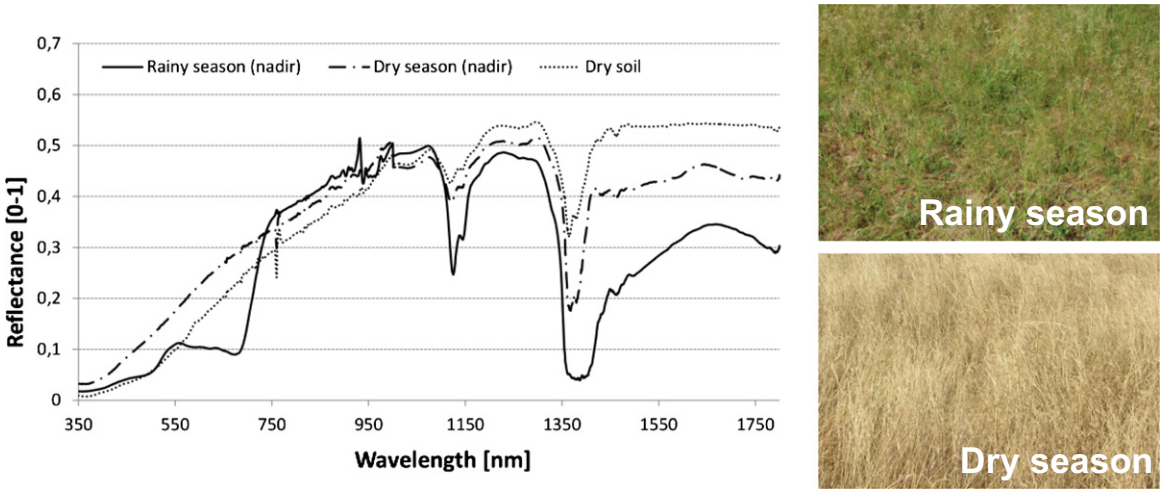

Fig. 5. Mean nadir spectra for the rainy season 2011 (DOY 237–251), the dry season 2012. (DOY 71–85) and dry soil 2013 (DOY 14).

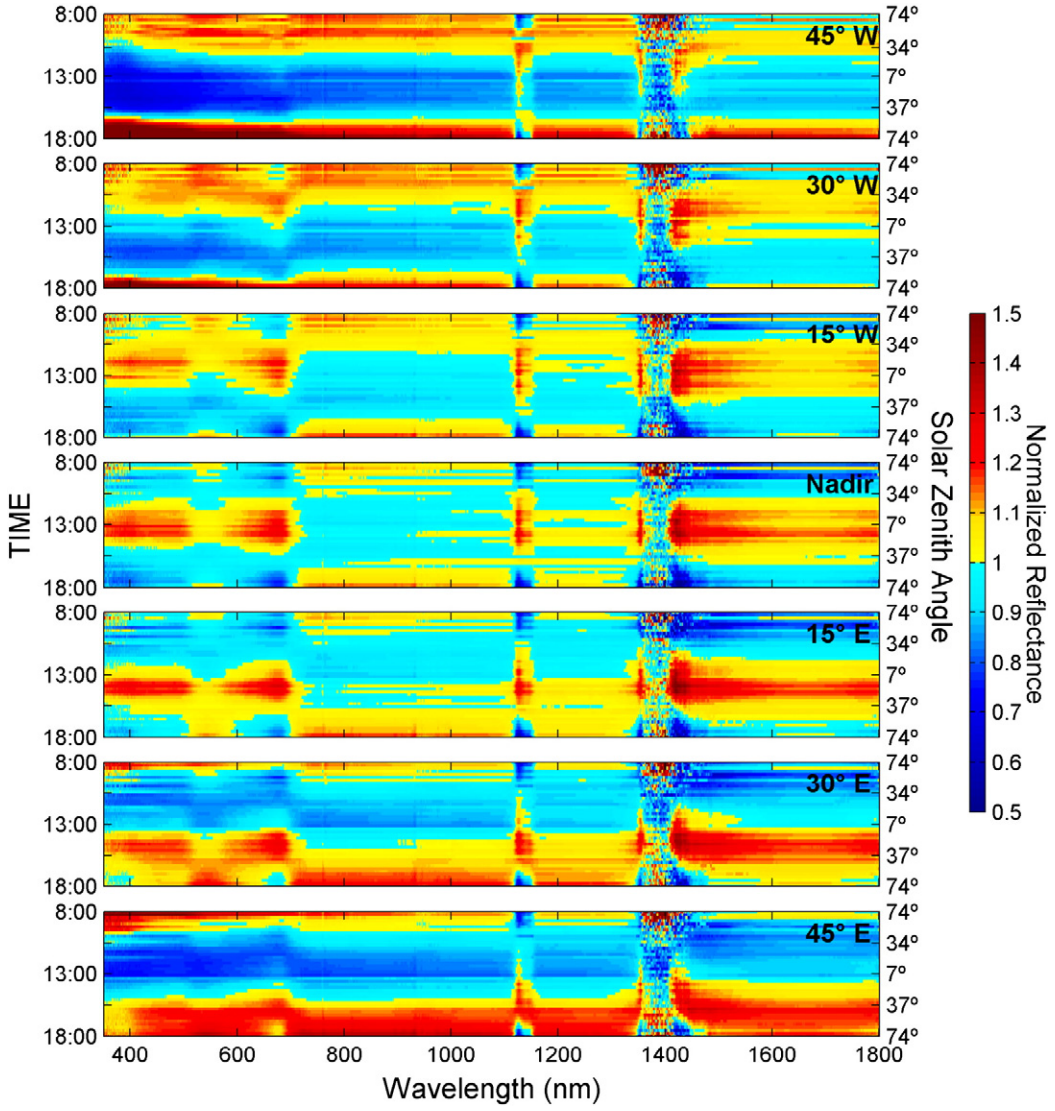

Fig. 6. Normalized reflectance (fraction of the time-specific reflectance spectra divided by the daily average) for the rainy season 2011 (DOY 237–251) measured from sunrise to sunset (solar noon is around 13:00). At the upper right corner of each figure the sensor view angle is indicated (e.g., 45° W: sensor measuring 45° off-nadir towards west). In the first three figures (15–45° W angles), in the morning, only back-scattered radiation reaches the sensor (solar irradiance from east) while forward-scattered radiation is measured by the sensor in the evening hours (solar irradiance from West). In the last three figures (15–45° E angles) the constellation is the other way round.

the atmosphere in the morning and the evening hours). This phenomenon is less evident in the data of the eastward-looking angles and is likely to be caused by shading from clumping of a group of trees (*Acacia Senegal*) located east of the tower (visible in the right part of the photo of Fig. 1). Another possible explanation could be diurnal changes within the atmosphere causing changes in the diffuse/direct radiation ratio. This has been reported for Senegal (Drame, Bilal, Camara, Sambou, & Gaye, 2012) where a strong diurnal fluctuation in the diffuse/direct radiation ratio (the diffuse radiation increasing in the afternoon) during the rainy season is observed due to the presence of cloud droplets. Finally, it could also be caused by heterogeneous ground vegetation affecting the reflectance measurements differently east and west of the tower.

Measurements during the dry season reveal much less anisotropic behavior as compared to the rainy season and more symmetric patterns regarding the eastward and westward-looking geometry, respectively (Fig. 7). The plants appear brownish and dry (Fig. 5) and accordingly the optical properties are completely changed. Only little irradiance is absorbed and therefore more radiation is available for scattering (Kimes, 1983) causing the surface reflectance to appear more isotropic. Also, the scattering processes are mainly affected by the canopy architecture which is assumed to be spectrally independent (Camillo, 1987) thereby producing wavelength independent normalized reflectance patterns over the course of the day. Only for the 30 and 45° off-nadir viewing angles pronounced forward scattering was measured in the morning and evening hours for eastward and westward looking directions, respectively. The geometric condition together with the waxy coatings of the plants might explain the extreme specular (mirror-like) surface reflectance observed in the data. The forward scattering is most distinctive in the VIS-NIR range, but also existent in the SWIR range.

3.3. Influence of spectral bandwidth on anisotropy of red, NIR and SWIR bands

In order to assess the influence of the spectral bandwidth on the target's anisotropy we compared the response of MODIS, SEVIRI and SPOT Vegetation sensors (resampled from ASD data). As can be seen in table 2, the bandwidths among the sensors vary considerably, with SEVIRI having the broadest bandwidths. However, there is almost no difference between the ANIFs for the different sensors (Fig. 8). For observations made during the rainy season (Fig. 8a), only SEVIRI's red band has slightly higher ANIF values for measurements for observation angles of 30° or larger as compared to MODIS and SPOT. This difference might be related to the bandwidth for red of SEVIRI which is much broader (150 nm) than for MODIS (50 nm) and SPOT (70 nm)

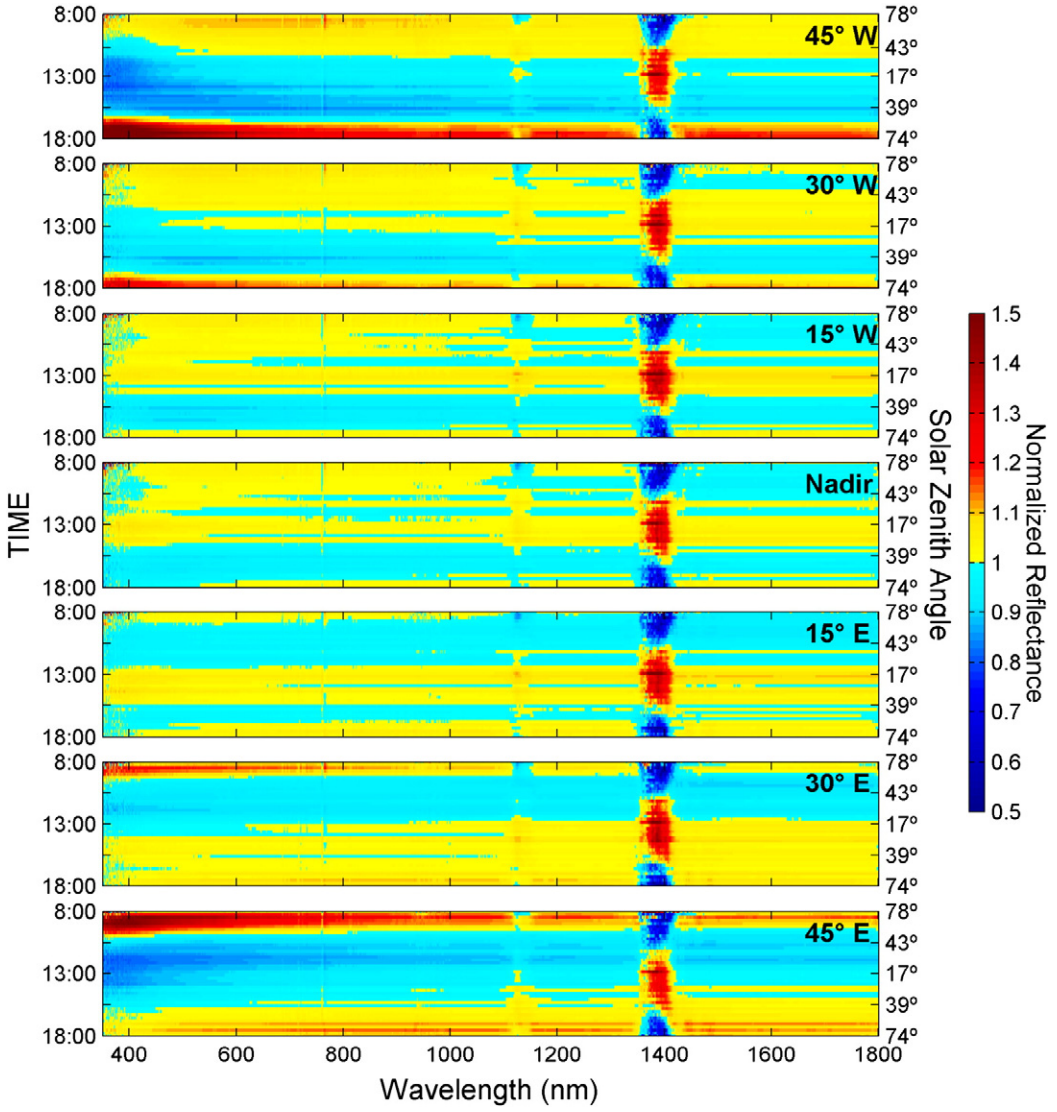

Fig. 7. Same as Fig. **5** but for the dry season 2012 (DOY 71–85) measured from sunrise to sunset (solar noon is around 13:00).

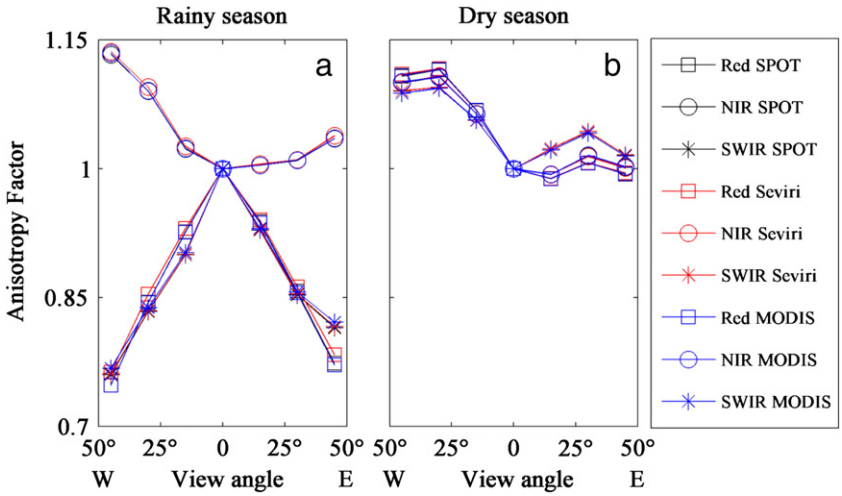

Fig. 8. Anisotropy factors for MODIS, SPOT and SEVIRI, respectively, obtained between 12:00 and 14:00: a) during the rainy season (DOY 237–251 2011) and b) during the dry season (DOY 71-85 2012).

(Table 2). Yet, a distinct difference in the general pattern appears for the rainy and dry season: during the rainy season, the ANIFs for the red and the SWIR bands show a similar shape since photosynthetically active leaves absorb irradiance in both wavelengths (chlorophyll and water respectively) while the NIR irradiance is mostly reflected or transmitted in the mesophyll of the plant material.

For the dry season observations (Fig. 8b), the ANIFs of all wavebands follow the same pattern; since there is no water and chlorophyll in the senescent plant material (limited absorption), the red and SWIR wavebands show the same pattern as the NIR. ANIFs are increasing with sensor viewing angle since more top of the vegetation canopy is viewed and soil and shading effects decreases (Kimes, 1983). However, at the 45° angle, the ANIFs are decreasing as compared to the ANIFs at 30°. It is clear in the ANIFs of both the dry and the rainy season that the patterns are not following the same shape in the eastern and the western direction as was also the case for the normalized reflectance in Figs. 6 and 7 which is likely to be caused by the distribution of trees and shrubs in the vicinity of the sensor field of view not being 100% uniform (natural savanna).

3.4. Influence of scattering direction on the reflectance of red, NIR and SWIR bands

In order to assess the influence of forward and backward scattering directions for the red, NIR and SWIR bands upon the target anisotropic behavior we analyzed the reflectance for these bands with a MODIS sensor configuration (resampled from ASD data) using median measurements from 9:00–10:00 for the dry (DOY 71–85) and rainy (DOY 237–251) seasons (Fig. 9) (also afternoon measurements could have been used). During morning hours forward and backward scattering is occurring for the measurements in the eastern and western directions, respectively (as shown in the normalized reflectance plots in Figs. 6 and 7). For all three spectral bands, higher reflectance was observed in the backward scattering direction as compared to the forward scattering direction, due to shading effects in the latter (Fig. 9). Also the characteristic bowl-shaped reflectance pattern as a function of the sensor viewing angle is present for all wavelengths during both the dry and rainy season as also found in (Deering, Eck, & Banerjee, 1999; Holben & Fraser, 1984; Huete, Hua, Qi, Chehbouni, & Vanleeuwen, 1992; Jin et al., 2002). However, this pattern is less distinctive for the SWIR during the rainy season as compared to red and NIR.

The effect of spectrally dependent anisotropic behavior of the savanna (Fig. 9) on vegetation indices like the Normalized Difference Vegetation Index (NDVI = NIR-Red/NIR + Red) and Shortwave Infrared Water Stress Index (SIWSI = NIR-SWIR/NIR + SWIR) is analyzed for the rainy season. As can be seen in Fig. 10, viewing angles have a strong impact on both vegetation indices with increasing index values for larger off-nadir viewing angles. The band specific reflectance differences for off nadir/nadir viewing geometry (red: 0.31–0.23 = 0.08; NIR: 0.57–0.43 = 0.13; SWIR: 0.31–0.23 = 0.08) produce different index values for off nadir/nadir viewing geometry (5 % difference for NDVI and 41 % for SIWSI). The especially pronounced view angle dependency for the SIWSI can be explained by the smaller difference in absolute reflectance values between the bands (NIR and SWIR). In the case of a vegetation cover that still allows the soil to be seen from the sensor, another contributing factor could be that the difference in SWIR reflectance between soil and vegetation is more pronounced than for red reflectance (Fig. 5). These findings are important for the evaluation of satellite based measurements where the disentangling between the impact from both viewing angle and the atmosphere can only be conducted from radiative transfer models (Holben & Fraser, 1984).

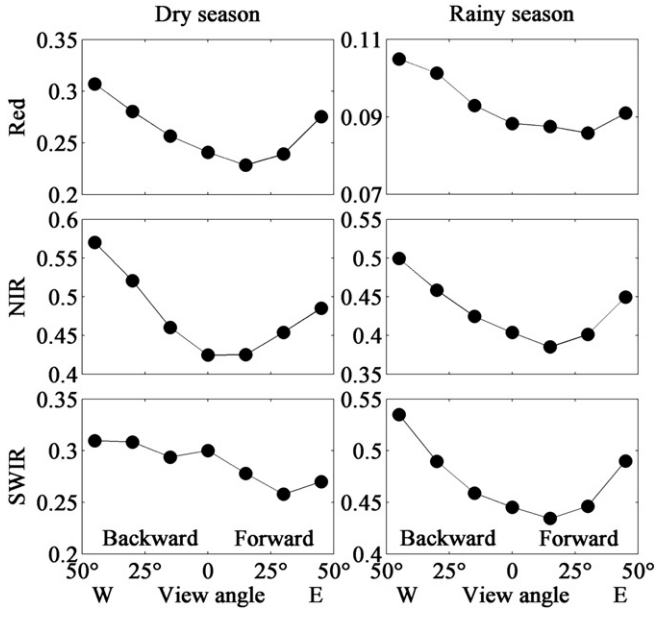

Fig. 9. Red, NIR and SWIR band reflectance (using the MODIS sensor configuration) for different viewing geometry obtained during the dry season (DOY 71-85 2012) (left) and rainy season (DOY 237-251 2011) (right). Values are calculated from the median of measured reflectances between 9:00 and 10:00 for the dry and rainy seasons, respectively.

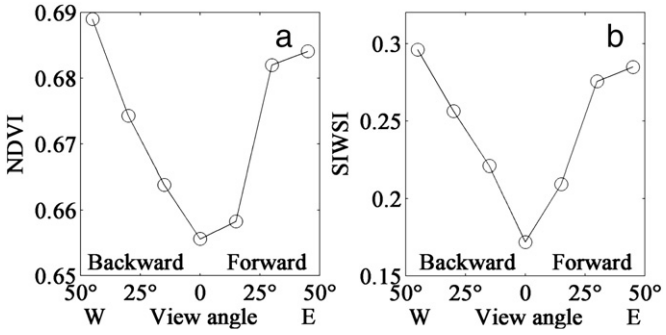

Fig. 10. (a) The Normalized Difference Vegetation Index (NDVI) and (b) the Shortwave Infrared Water Stress Index (SIWSI) for different sensor viewing geometries. Red, NIR and SWIR band reflectance (using the MODIS sensor configuration) for different viewing geometry obtained during the rainy season (DOY 237-251 2011). Values are calculated from the median of measured reflectances between 9:00 and 10:00.

Many satellite remote sensing based studies have pointed out the problem of band specific differences in the BRF causing NDVI to increase in the forward scatter direction because of shading effects being more pronounced in the red part of the spectrum as compared to NIR (e.g., Cihlar, Manak, & Voisin, 1994; Fensholt, Huber, Proud, & Mbow, 2010; Fensholt, Sandholt, Proud, Stisen, & Rasmussen, 2010; Gao, Jin, Schaaf, & Strahler, 2002) when using a maximum compositing approach (Holben, 1986) and for an erectophile canopy structure like savanna in particular (Goel & Kong, 1989). Also *in situ* based measurements from semi-arid grassland (Huete et al., 1992) have shown NDVI sensitivity to directional effects. Surprisingly, Fig. 10 shows that both NDVI and SIWSI produce similar index values in the eastern (forward scatter) and western (backward scatter) direction, indicating that the band specific effects of backward and forward scattering (Fig. 9) cancel out during the index calculations. The observed difference between forward and backward scatter direction reflectance (in Fig. 9) is compensated for in the index calculation by the band specific differences in the absolute level of reflectance values, thereby producing almost identical NDVI and SIWSI index values in the forward and backward scatter direction (0.2 % NDVI difference and 0.5 % SIWSI difference between forward and backward scatter directions (avg. of 15, 30 and 45° angles)).

4. Conclusions/Outlook

First data from the Dahra field spectrometer system reveal significant differences between measurements taken during the rainy and dry season. We observed much more pronounced anisotropy for measurements taken above a green vegetation canopy as compared to the dry season. The complex radiative processes within a green canopy with absorption, reflection, multiple scattering led to distinctive patterns for the VIS, NIR and SWIR. We found most pronounced patterns for the VIS and SWIR ranges, where green plants (chlorophyll and water) absorb large parts of the incoming radiation as compared to a dry vegetation canopy. When comparing reflectance data resampled to MODIS, SPOT and SEVIRI sensor configurations, the ANIFs per band were very similar for the different sensors, indicating that differences in spectral bandwidths do not influence much the anisotropic behavior of savanna. Yet, satellite based measurements from different sensors also imply changing GIFOVs which influence the measured reflectance. Vegetation indices including red/NIR (NDVI) and NIR/SWIR (SIWSI) were found to be sensitive to the view angle with the influence on NIR/SWIR being most severe (5 % difference for NDVI and 41 % for SIWSI). However, for savanna no influence on vegetation indices was found as a function of forward vs. backwards scatter directions (0.2 % and 0.5 % difference for NDVI and SIWSI, respectively).

Ground-based measurements of wavelength-dependent anisotropy of surface reflectance for a savanna landscape during different phenological stages are crucial for understanding the accuracy/uncertainty related to traditional EO-based vegetation indices but also for the development of new indices and algorithms e.g. including SWIR based water stress. Foreseen is also research related to upscaling studies including spectroradiometers mounted on Unmanned Aerial Vehicles for inter-comparison of hyperspectral reflectance data with carbon flux measurements conducted at the Dahra site. The optical data measured at 15-minute time intervals are very well suited to be compared with highly variable water and carbon fluxes between the biosphere and the atmosphere that are typical for tropical water limited savanna landscapes.

At present very few radiometers on the market cover wavelengths beyond NIR because of the different instrumental requirements for SWIR. The ASD instruments used at the Dahra site covering VIS/NIR/SWIR are very costly and actually not designed for fully automatic continuous outdoor recordings. Measurements at the Dahra site were initiated in 2011 and the remote controlling of the instruments using scripting language causes no problems. However, several periods of ASD malfunctioning have encountered over the three years of operation. Occasionally, the problem could be solved from local support (computer restarting etc.), but shipping of the instruments to the manufacturer was also frequently required being time consuming; in general, the ASD based system has shown to be quite costly. The environment in which the DAFIS is operating is very harsh with highly variable temperatures and high loads of dust in the atmosphere during the dry season. Considering this challenge, a more low-tech, reliable and cheaper system providing the same spectral configuration would be preferable.

Acknowledgments

We are thankful to the three reviewers for their helpful comments which contributed to improve this manuscript. We would also like to thank all the individuals involved in the field campaigns in Senegal as well as the maintenance and management of the Dahra field station. This research is part of the project entitled Earth Observation based Vegetation productivity and Land Degradation Trends in Global Drylands. The project is funded by the Danish Council for Independent Research (DFF) Sapere Aude program.

References

Analytical Spectral Devices, Inc. (ASD) (1999). Technical Guide. In David C. Hatchell (Ed.), *Analytical Spectral Devices, Inc* (4th ed.). CO, USA: Boulder.

Camillo, P. (1987). A Canopy Reflectance Model Based on an Analytical Solution to the Multiple-Scattering Equation. *Remote Sensing of Environment*, *23*(3), 453–477.

Carter, G. A. (1991). Primary and Secondary Effects of Water-Content on the Spectral Reflectance of Leaves. *American Journal of Botany*, *78*(7), 916–924.

Ceccato, P., Flasse, S., Tarantola, S., Jacquemoud, S., & Grégoire, J. -M. (2001). Detecting vegetation leaf water content using reflectance in the optical domain. *Remote Sensing of Environment*, *77*(1), 22–33.

Cihlar, J., Manak, D., & Voisin, N. (1994). AVHRR bidirectional reflectance effects and compositing. *Remote Sensing of Environment*. http://dx.doi.org/10.1016/0034-4257(94)90116-3.

Deering, D. W., Eck, T. F., & Banerjee, B. (1999). Characterization of the reflectance anisotropy of three Boreal forest canopies in spring-summer. *Remote Sensing of Environment*, *67*, 205–229. http://dx.doi.org/10.1016/S0034-4257(98)00087-X.

Diallo, O., Diouf, A., Hanan, N. P., Ndiaye, A., & Prévost, Y. (1991). AVHRR monitoring of savanna primary production in Senegal, West Africa: 1987–1988. *International Journal of Remote Sensing*. http://dx.doi.org/10.1080/01431169108929725.

Drame, M., Bilal, B. O., Camara, M., Sambou, V., & Gaye, A. (2012). Impacts of aerosols on available solar energy at Mbour, Senegal. *Journal of Renewable and Sustainable Energy*, *4*.

Fensholt, R., Huber, S., Proud, S. R., & Mbow, C. (2010). Detecting Canopy Water Status Using Shortwave Infrared Reflectance Data From Polar Orbiting and Geostationary Platforms. *IEEE Journal of Selected Topics in Applied Earth Observations and Remote Sensing*. http://dx.doi.org/10.1109/JSTARS.2010.2048744.

Fensholt, R., & Sandholt, I. (2003). Derivation of a shortwave infrared water stress index from MODIS near- and shortwave infrared data in a semiarid environment. *Remote Sensing of Environment*, *87*(1), 111–121.

Fensholt, R., & Sandholt, I. (2005). Evaluation of MODIS and NOAA AVHRR vegetation indices with in situ measurements in a semi-arid environment. *International Journal of Remote Sensing*, *26*, 2561–2594. http://dx.doi.org/10.1080/01431160500033724.

Fensholt, R., Sandholt, I., Proud, S. R., Stisen, S., & Rasmussen, M. O. (2010). Assessment of MODIS sun-sensor geometry variations effect on observed NDVI using MSG SEVIRI

geostationary data. *International Journal of Remote Sensing*. http://dx.doi.org/10.1080/01431160903401387.
Fensholt, R., Sandholt, I., & Stisen, S. (2006). Evaluating MODIS, MERIS, and VEGETATION — Vegetation indices using in situ measurements in a semiarid environment. *IEEE Transactions on Geoscience and Remote Sensing*, *44*(7), 1774–1786. http://dx.doi.org/10.1109/tgrs.2006.875940.
Gamon, J. A., Cheng, Y. F., Claudio, H., MacKinney, L., & Sims, D. A. (2006). A mobile tram system for systematic sampling of ecosystem optical properties. *Remote Sensing of Environment*, *103*(3), 246–254. http://dx.doi.org/10.1016/j.rse.2006.04.006.
Gamon, J. A., Rahman, A. F., Dungan, J. L., Schildhauer, M., & Huemmrich, K. F. (2006). Spectral Network (SpecNet) — What is it and why do we need it? *Remote Sensing of Environment*, *103*(3), 227–235. http://dx.doi.org/10.1016/j.rse.2006.04.003.
Gao, B. C. (1996). NDWI — A normalized difference water index for remote sensing of vegetation liquid water from space. *Remote Sensing of Environment*, *58*(3), 257–266.
Gao, F. G. F., Jin, Y. J. Y., Schaaf, C. B., & Strahler, A. H. (2002). Bidirectional NDVI and atmospherically resistant BRDF inversion for vegetation canopy. *IEEE Transactions on Geoscience and Remote Sensing*, *40*. http://dx.doi.org/10.1109/TGRS.2002.800241.
Goel, N. S., & Kong, J. A. (1989). Inversion of Canopy Reflectance Models for Estimation of Biophysical Parameters from Reflectance Data. In G. Asrar (Ed.), *Theory and Applications of Optical remote Sensing* (pp. 205–251). Washington, D.C.: Wiley.
Govaerts, Y. M., Jacquemoud, S., Verstraete, M. M., & Ustin, S. L. (1996). Three-dimensional radiation transfer modeling in a dicotyledon leaf. *Applied Optics*, *35*(33), 6585–6598. http://dx.doi.org/10.1364/Ao.35.006585.
Grant, L. (1987). Diffuse and specular characteristics of leaf reflectance. *Remote Sensing of Environment*, *22*(2), 309–322. http://dx.doi.org/10.1016/0034-4257(87)90064-2.
Hanan, N. P., Prevost, Y., Diouf, A., & Diallo, O. (1991). Assessment of desertification around deep wells in the Sahel using satellite imagery. *Journal of Applied Ecology*, *28*, 173–186. http://dx.doi.org/10.2307/2404123.
Hapke, B., DiMucci, D., Nelson, R., & Smythe, W. (1996). The cause of the hot spot in vegetation canopies and soils: Shadow-hiding versus coherent backscatter. *Remote Sensing of Environment*, *58*(1), 63–68.
Hilker, T., Coops, N. C., Nesic, Z., Wulder, M. A., & Black, A. T. (2007). Instrumentation and approach for unattended year round tower based measurements of spectral reflectance. *Computers and Electronics in Agriculture*, *56*(1), 72–84. http://dx.doi.org/10.1016/j.compag.2007.01.003.
Hilker, T., Nesic, Z., Coops, N. C., & Lessard, D. (2010). A new, automated, multiangular radiometer instrument for tower-based observations of canopy reflectance (AMSPEC II). *Instrumentation Science and Technology*, *38*(5), 319–340.
Holben, B. (1986). Characteristics of maximum-value composite images from temporal AVHRR data. *International Journal of Remote Sensing*, *7*(11), 1417–1434. http://dx.doi.org/10.1080/01431168608948945.
Holben, B., & Fraser, R. S. (1984). Red and near-infrared sensor response to off-nadiir viewing. *International Journal of Remote Sensing*, *5*(1), 145–160. http://dx.doi.org/10.1080/01431168408948795.
Huete, A. R., Hua, G., Qi, J., Chehbouni, A., & Vanleeuwen, W. J. D. (1992). Normalization of Multidirectional Red and Nir Reflectances with the Savi. *Remote Sensing of Environment*, *41*(2–3), 143–154.
Jacquemoud, S., Verhoef, W., Baret, F., Bacour, C., Zarco-Tejada, P. J., Asner, G. P., François, C., & Ustin, S. L. (2009). PROSPECT + SAIL models: A review of use for vegetation characterization. *Remote Sensing of Environment*. http://dx.doi.org/10.1016/j.rse.2008.01.026.
Jin, Y. J. Y., Gao, F. G. F., Schaaf, C. B., Li, X. L. X., Strahler, A. H., Bruegge, C. J., & Martonchik, J. V. (2002). Improving MODIS surface BRDF/Albedo retrieval with MISR multiangle observations. *IEEE Transactions on Geoscience and Remote Sensing*, *40*. http://dx.doi.org/10.1109/TGRS.2002.801145.
Kandji, S. T., Verchot, L., & Mackensen, J. (2006). Climate change and variability in the Sahel region: impacts and adaptation strategies in the agricultural sector. *Environment*, 48.
Kimes, D. S. (1983). Dynamics of Directional Reflectance Factor Distributions for Vegetation Canopies. *Applied Optics*, *22*(9), 1364–1372.
Kimes, D. S. (1984). Modelling the directional reflectance from complete homogeneous vegetation canopies with various leaf-orientation distributions. *Journal of the Optical Society of America A: Optics and Image Science, and Vision*, *1*(7), 725–737.
Latifovic, R., Cihlar, J., & Chen, J. C. J. (2003). A comparison of BRDF models for the normalization of satellite optical data to a standard Sun-target-sensor geometry. *IEEE Transactions on Geoscience and Remote Sensing*, *41*. http://dx.doi.org/10.1109/TGRS.2003.811557.
Leuning, R., Hughes, D., Daniel, P., Coops, N. C., & Newnham, G. (2006). A multi-angle spectrometer for automatic measurement of plant canopy reflectance spectra. *Remote Sensing of Environment*, *103*(3), 236–245. http://dx.doi.org/10.1016/j.rse.2005.06.016.
Lucht, W., Schaaf, C. B., & Strahler, A. H. (2000). An algorithm for the retrieval of albedo from space using semiempirical BRDF models. *IEEE Transactions on Geoscience and Remote Sensing*, *38*. http://dx.doi.org/10.1109/36.841980.
Nemani, R. R., Keeling, C. D., Hashimoto, H., Jolly, W. M., Piper, S. C., Tucker, C. J., & Running, S. W. (2003). Climate-driven increases in global terrestrial net primary production from 1982 to 1999. *Science (New York, N.Y.)*, *300*, 1560–1563. http://dx.doi.org/10.1126/science.1082750.
Nicholson, S. E., Dezfuli, A. K., & Klotter, D. (2012). A Two-Century Precipitation Data Set for the Continent of Africa. *Bulletin of the American Meteorological Society*. http://dx.doi.org/10.1175/BAMS-D-11-00212.1.
Privette, J. L., & Vermote, E. (2004). The impact of atmospheric effects on directional reflectance measurements. In M. v. Schoenermark, B. Geiger, & H. P. Roeser (Eds.), *Reflectance Properties of vegetaiton and Soil* (pp. 225–241). Berlin: Wissenschaft und Technik Verlag.
Ridder, N., Stroosnijder, L., Cisse, A. M., & van Kelulen, H. (1982). *Productivity of Sahelian rangeland, a study of the soils, the vegetation and the exploitation of the natural resources: PPS course book*. Wageningen, The Netherlands: Wageningen Agricultural University, Dept. of Soil Science and Plant Nutrition.
Sandmeier, S., Muller, C., Hosgood, B., & Andreoli, G. (1998). Physical Mechanisms in Hyperspectral BRDF Data of Grass and Watercress. *Remote Sensing of Environment*, *66*(2), 222–233. http://dx.doi.org/10.1016/S0034-4257(98)00060-1.
TMCL™ firmware manual (d). http://www.mocontronic.de/files/TMCM-1110_TMCL_firmware_manual.pdf (accessed 22 March 2014)
Tucker, C. J. (1980). Remote-Sensing of Leaf Water-Content in the near-Infrared. *Remote Sensing of Environment*, *10*(1), 23–32.
Valenza, J., & Diallo, A. K. (1972). Etude des pâturages naturels du nord Sénégal. *Rapport et Cartes: Etude Agrostologique I.E.M.V.T.*
Walthall, C., Roujean, J. L., & Morisette, J. (2000). Field and landscape BRDF optical wavelength measurements: Experience, techniques and the future. *Remote Sensing Reviews*, *18*(2), 503–531.
Wang, L., & Qu, J. J. (2007). NMDI: A normalized multi-band drought index for monitoring soil and vegetation moisture with satellite remote sensing. *Geophysical Research Letters*. http://dx.doi.org/10.1029/2007GL031021.
Wang, L., Qu, J. J., Hao, X., & Zhu, Q. (2008). Sensitivity studies of the moisture effects on MODIS SWIR reflectance and vegetation water indices. *International Journal of Remote Sensing*. http://dx.doi.org/10.1080/01431160802226034.
Weyermann, J., Damm, A., Kneubühler, M., & Schaepman, M. E. (2013). Correction of Reflectance Anisotropy Effects of Vegetation on Airborne Spectroscopy Data and Derived Products. *Geoscience and Remote Sensing, IEEE Transactions on*, *PP(99)*, 1–12. http://dx.doi.org/10.1109/tgrs.2013.2242898.
Zarco-Tejada, P. J., Rueda, C. A., & Ustin, S. L. (2003). Water content estimation in vegetation with MODIS reflectance data and model inversion methods. *Remote Sensing of Environment*, *85*(1), 109–124. http://dx.doi.org/10.1016/S0034-4257(02)00197-9.
Zhao, S. H., Wang, Q., Zhang, F., Yao, Y. J., Qin, Q. M., You, L., & Li, Y. (2013). Drought Mapping Using Two Shortwave Infrared Water Indices with MODIS Data under Vegetated Season. *Journal of Environmental Informatics*, *21*, 102–111.